Back to Session Subjects

HELIFLOW PITCH-UP AND QUARTERING FLIGHT EXPERIMENTS.

I W Kaynes (DERA), G Preatoni (Agusta), A Visingardi and N Tino (CIRA) , C Arzoumanian (Eurocopter), K Kampa (ECD), C. Hermans and B.S.M. Renier (NLR) , F Tchen-Fo and N Bettschart (ONERA), R Harrison (GKN-WHL)

Abstract

The paper describes two tasks of the European collaborative project HELIFLOW which addressed the low speed phenomena of pitch-up and quartering flight. Both tasks included experimental investigations in the DERA 24ft wind tunnel and analysis and predictions by all partners.

The pitch-up test employed a generic streamlined helicopter fuselage designed by Agusta with four mounting locations for the tailplane. The fuselage was mounted on the DERA rotor test rig and tested from hover up to an advance ratio of 0.1. Data were obtained on rotor characteristics and fuselage and tailplane aerodynamic pressures forces and moments. Flow measurements were undertaken by CIRA using PIV and hot wire anemometry.

The quartering flight test used a tail rotor made by GKN-Westland mounted on an independent stand and moveable relative to the DERA main rotor rig. Tail rotor and main rotor characteristics were measured with the tail rotor at azimuth positions between zero and 70^{o}, at two vertical locations and with both directions of tail rotor rotation.

This paper gives an overview of the experiments and a summary of results obtained by the HELIFLOW partners. Analyses were conducted by each partner and fell into two categories, flight mechanics codes or detailed flow prediction methods.

NLR contributed to the analysis activities by performing flight mechanics related aerodynamic load calculations with the commercial software tool FlightLab. The analysis focussed on the validation of the rotor (dynamic) wake interaction module. First the isolated main and tail rotor model characteristics were checked against the experimental data. Next the wake interaction behaviour performance was verified. The correlation of the stabiliser normal force at aft positions, which has a major impact on the pitch-up behaviour of the helicopter, was especially good.

ONERA used the vortex rings model for the main rotor wake with the simulation tool HOST. Calculating the tailplane force by using flow velocity at two chordwise positions on the tailplane gave a change of lift in agreement with the experiment. ONERA also made computations using the PEIRF code for the complete rotor plus fuselage model. Wake trajectories were found and comparisons made with pressure measurements on the fuselage.

Eurocopter used the simulation tool HOST with an empirical interaction model to calculate the mean induced velocity on the tailplane and also at the tail rotor location. Improvements were implemented concerning the empirical model wake contraction and entry and exit of the wake. The predicted build up of tailplane normal force against advance ratio was slower than shown by the data for the most forward tailplane position but in good agreement for the rear tail positions.

DERA applied a free wake model to the prediction of the wake velocities in the vicinity of the tailplane and tail rotor. The vortex core trajectories have been compared to the PIV measurements and the tailplane forces evaluated.

CIRA and Agusta made flow predictions with RAMSYS and evaluated wake development, wake boundary and pressures on the model.

1 Introduction

The experiments described in this paper were undertaken as part of Brite/Euram III project HELIFLOW BRPR-CT96-0206. The project objective was to improve experimental and theoretical tools for helicopter aeromechanic and aeroacoustic interactions. There were six experimental tasks in the project and two of these are the subject of this paper.

Pitch-Up and Quartering Flight are two phenomena which can give rise to difficulties in the flight test programme of a new helicopter as a result of inadequacies in the prediction of low speed interactional flow. The HELIFLOW tasks studying these interactions both included a low speed wind tunnel experiment set up to simulate the fundamental characteristics and the application of this data for the validation and improvement of prediction codes. The partners involved in both tasks were Agusta, DERA, Eurocopter, GKN-Westland, NLR and ONERA, plus CIRA participating in the pitch-up task.

2 Pitch-Up

2.1 Introduction

During the transition from hover to forward flight a helicopter undergoes changes in pitching moment caused by the interaction of the main rotor wake with the tailplane. In hover the tailplane is usually behind the rotor wake but as forward speed is built up the wake moves back to impinge on the tailplane and produce a significant nose-up pitching moment. Errors in prediction of the phenomenon can result in expensive modifications of tailplane position or geometry and related extra flight test time during development of a helicopter.

2.2 Configuration of experiment

The HELIFLOW pitch-up experiment employed a generic streamlined helicopter fuselage which was designed by Agusta, ref.1. Rather than use a specific scale model fuselage, the generic design was aimed at avoiding flow separations and other specific characteristics which might mask the pitch-up or hinder the generalisation of the results. The fuselage included a fixed fin and had provision for mounting a single-sided or symmetric tailplane at four different locations (fig.1)

The fuselage was fitted to the DERA rotor test rig on which was mounted a 3m diameter rotor with four rectangular blades, ref.2,3. The fuselage was tilted forward by 4^o relative to the rotor rig and the tailplane was mounted at -4^o incidence on the fuselage, so that the tailplane was horizontal when the rotor shaft was vertical. Tests were conducted with the rotor rig at 2^o and 4^o tilt.

The complete model (fig.2) was tested at DERA Farnborough in the hover site and the 24ft open jet wind tunnel. Tests were conducted at a range of advance ratio from hover up to 0.1 with the rotor operating at Mach scaled conditions (1400 rpm). Two thrusts were studied, CT/σ=0.08 and 0.1, and the rotor was trimmed to zero-flapping for most tests and with some additional tests with a flight mechanics trim attempting to simulate the trim balance of a hypothetical real helicopter. The tests were summarised in ref.4.

Data were obtained from rotor, fuselage and tailplane load balances, rotor control settings, blade strain gauges. Surface pressures were measured with 87 unsteady pressure transducers on the upper fuselage and tail boom and on upper and lower surfaces of the tailplane, as shown in fig.3. Flow measurements were undertaken by CIRA using Particle Image Velocimetry (PIV) and Hot Wire Anemometry (HWA).

In addition AGUSTA had undertaken wind tunnel tests on the isolated tailplane for a full range of incidence to assess its aerodynamic characteristics.

2.3 Experimental results

2.3.1 Flow measurements

The flow field in the vicinity of the tailplane is a direct indication of the cause of pitch-up. The flow was measured by CIRA with two complementary techniques PIV and HWA, the latter including both a 2-D probe on a traverse and glue-on surface probes, ref.5, 6, 7.

The most interesting conditions were identified by initial observation of the behaviour of tailplane normal force as described in the following section. Detailed flow measurement was then concentrated on these conditions, that is tail positions 2 and 3, advance ratio from 0.015 to 0.05 and one shaft angle (2^o). During these tests the tailplane was removed from the fuselage, in order to facilitate observation of the baseline flow from the rotor in a region covering the tailplane location and directly in front of the tailplane.

For PIV the camera was mounted 7m from the wind tunnel centre-line at the same height as the tailplane. The observation plane was in line with the spanwise location of the outer row of pressure transducers on the left tailplane. For both tailplane positions images were obtained at two zones, one in front of the tailplane and the other enclosing it. The two zones for tailplane position 3 are shown in fig.4 .The particle motion in each image of a zone was processed to produce an array of 79 x 63 pairs of u and w components of velocity. A sample view of velocities derived from a PIV image is shown in fig.5. Note in this view the instantaneous position of the vortex shed by the main rotor tip: the vortex is directly above the position which had been occupied by the tailplane leading edge, implying a significant interaction .

Fig.6 shows the location of the most intense vortices seen in the sets of images from four PIV tests for advance ratio 0.03. The different symbols correspond to different image locations, the boundaries of which are shown by the thin line boxes. It is seen that for this condition the vortices are concentrated in the region of the leading edge of tailplane position 2

HWA measurements of u and w components of velocity were made with a 2-D probe along a traverse in the direction parallel to the wind tunnel flow direction. The traverse path was located at the same spanwise distance from the fuselage centre line as that used for the PIV, but in this case sets of readings were taken on both sides of the helicopter. The vertical location of the HWA path was through the position of the quarter chord of the tailplane. The traverse movement extended from 0.20m in front of a leading edge position to the trailing edge location, a total range of 0.35m. A CIRA data acquisition system with high sampling rate (28320 Hz) was used to record the HWA data with adequate detail to show the passage of vortices.

Additional measurements were made with glue-on probes on the tailplane and on the fuselage in the vicinity of the tailplane. This HW system allows the immediate detection of the boundary layer condition as attached or separated. Data from the tailplane confirm separated flow on the underside of the tailplane in position 2 in pitch-up conditions of advance ratio 0.04.

Within part of the HWA traverse range there was also the possibility to extract the velocity components from a corresponding section across the PIV images, ref.8. These mean velocity component profiles are compared in figures 7 and 8 for an advance ratio 0.03. Using data from a full complement of zones and tailplane locations, these plots include four sets of velocities derived from PIV and two sets for HWA. It is seen that the vertical velocities from each source are closely self-consistent but there is a difference between the PIV and HWA, corresponding to a horizontal shift of wake location of about 0.05m. Analysis suggests that a possible cause of the difference could have been aerodynamic interference from the traverse affecting the HWA data. The horizontal components from HWA and PIV are very similar but subject again to a slight shift of the wake boundary. Similar behaviour was found when examining other advance ratios.

2.3.2 Tailplane normal force measurements

The most direct indication of pitch-up is given by the evolution of tail plane normal force with the increase of advance ratio. This is shown in figure 9 for each tailplane position.

It is seen that at the most forward position, SYM1, the tailplane carries a considerable download even at the lowest advance ratio of 0.015. This position had the tailplane quarter-chord on the fuselage centre-line about 83% of rotor radius behind the hub.

Position SYM2 had the quarter chord at 96% of rotor radius and in this case the down force on the tail is small at the slowest advance ratio, indicating that the rotor wake contraction has not been offset by forward speed and the bulk of the tailplane remains outside the wake. As advance ratio increases there is a rapid increase in download up to full immersion in the wake at μ=0.08.

SYM3, the furthest aft fuselage position for the tailplane, has the tail almost unaffected at advance ratio below 0.03. As speed increases above this value the download continues to increase and at μ=0.10 the force reaches the greatest seen for any tailplane position. PORT3 represents the asymmetric tailplane at position 3, only on the port side but with a span extension. It is seen that the force increase with advance ratio follows the same trend as seen for SYM3.

The final tailplane position, SYM4, was slightly to the rear of SYM3 but mounted at mid-height on the fin. There is little load on the tailplane for advance ratio up to 0.04, followed by an increase in download which is an initially quite gradual.

The data confirms that pitch-up occurs at higher speeds for more rearward location of the tailplane and it also shows that the peak contribution to pitching moment also increases with more rearward tail positions.

Longitudinal force (drag) on the tailplane was also measured but in general this quantity is less significant in pitch-up than the normal force.

2.4 Prediction methods

Each partner in the project applied their own prediction techniques to simulation of pitch-up and these are briefly summarised in this section and in ref.9. The methods fall into two general categories, flight mechanics and detailed flow prediction codes

In the first category, NLR contributed to the analysis activities by performing flight mechanics related aerodynamic load calculations with the commercial software tool FlightLab. The analysis focussed on the validation of the rotor (dynamic) wake interaction module. First the isolated main rotor characteristics were checked against the experimental data. Next the wake interaction behaviour performance was verified (ref.10).

ONERA used the vortex rings model for the main rotor wake with the simulation tool HOST. Eurocopter, ref.11, and ECD, ref.12, used the simulation tool HOST with an empirical interaction model to calculate the mean velocity on the tailplane and also at the tail rotor location.

GKN Westland, ref.13, used a simple 2D model derived on the basis of momentum theory to predict the downwash at the tailplane for specified shaft tilts and thrusts.

In the analytical category of predictions, DERA applied a free wake model to the prediction of the wake velocities in the vicinity of the tailplane.

ONERA made computations using the PEIRF code for the complete rotor plus fuselage model.

CIRA and Agusta made flow predictions with RAMSYS, an unsteady panel method modelling of the fuselage and rotor and incorporating a free wake model. Agusta also used the VSAERO panel method steady aerodynamics code for studies of fuselage pressure.

2.5 Comparisons with predictions

2.5.1 Aeromechanics predictions

Prediction of the interacting flow is a fundamental aspect of all the prediction methods applied by partners. Detailed flowfield calculations are required for calculations of phenomena such as vibration and acoustics while for overall vehicle stability and control a less detailed averaged prediction is more appropriate.

Aeromechanics codes in general use mean induced velocity predictions from wake modelling based on momentum theory for the rotor, a trapezoidal inflow velocity distribution, and angles defining the wake skew angles. The parameters of such a model may be defined from geometry and flow properties or from previous empirical fitting. After some test measurements have been made it is possible to refine the parameters to better model the specific experiment. An example of the resulting simplified mean velocity distribution predicted at the tailplane is demonstrated by the GKN-Westland result shown in fig.10.

An initial stage of code application is to validate the basic rotor parameters. Partners obtained generally close agreement on the rotor thrust, torque, moments, side forces and angles measured on the rotor rig.

The natural outcome of aeromechanics codes applications is the prediction of the load on the tailplane, which in turns applies a pitching moment to the aircraft. A demonstration of the improvement of interaction model with fitting the parameters for the HELIFLOW test is shown in fig.11.

A combination of predictions by a number of partners are presented in fig.12 to 15 for the range of tailplane positions. Note that these results are total force for the complete tailplane on both sides of the fuselage. Some of the codes do not include asymmetric variation of the wake.

It is seen that the most forward tailplane position, SYM1, is predicted best by the ECD method as improved for this test data. The other two results do not show the tailplane immersed in the wake at the lowest advance ratio.

For the more usual rearward locations of the tailplane, the predictions are generally closer to the measurements. At position SYM2 the most of the codes give an initial build-up of tail force between 0.02 and 0.04 which is less rapid than the wind tunnel data, i.e. predicting a less abrupt entry to pitch-up than was measured. Final force magnitude at the highest advance ratio, when the tailplane has fully entered the wake, is well predicted by two codes and slightly under-predicted by the other two.

For the rearmost tail positions SYM3 and SYM4 the predictions lie around the measured data for most speeds.

In conclusion, the codes predict the general characteristics of pitch-up, but in specific circumstances there may be some differences. These could lead to some problems at the flight test stage of a completely new helicopter.

Code improvements as a result of validation against the HELIFLOW results include:

> Calculating the tailplane force by using flow velocity at two chordwise positions on the tailplane gave better agreement with the experiment than a single chordwise position.
>
> Improvements were made to the empirical model wake contraction and entry and exit angles of the wake.

2.5.2 Flowfield predictions

AGUSTA carried out predictions of the pressure distribution over the fuselage and tailplane using the VSAERO steady code. Analyses of a clean configuration without the rotor and hub showed the baseline pressures and tailplane forces on the vehicle. The tailplane normal forces were investigated for a range of incidence (model tilted on the shaft) when the rotor hub had been added to the VSAERO representation. The results were close to the measured values. A rotor was added to the simulation and

detailed studies made of wake geometry and flow velocities. The mean tailplane normal forces were near to the wind tunnel test values.

The VSAERO modelling geometry was used as a basis for the AGUSTA application of the RAMSYS unsteady aerodynamics simulation, ref.14. RAMSYS was also used by CIRA, ref.15. Application of RAMSYS in these predictions is limited by the presence of areas of separated flow.

The RAMSYS studies at low advance ratio examined the development of the rotor free wake, the wakes of the tailplane, the time histories of pressure distributions at the transducer locations, rotor thrust, and velocities at the PIV plane. A sample of the trajectories of the tip vortices is shown in fig.16. The predicted wake location was found to be further aft than measured. The pressure comparisons were restricted by questions about the calibration of the pressure transducers and the applicability of the code for regions of separated flow, but the results were in general qualitative agreement with good phase accuracy, as shown for example in fig.17. Evaluations of tailplane normal force at low speed gave consistent trends but with amplitude rather low.

CIRA also applied RAMSYS to a test case at advance ratio 0.1, the highest speed used in the test. The same test condition was also studied by ONERA with the PEIRF code, with this condition chosen to aid convergence of the code, although above the onset of pitch-up. The rotor wake boundaries predicted by the two codes are shown in fig.18 and the tip vortex circulation in fig.19. The pressures predicted on the fuselage by PEIRF are closer to the experiment (fig.20), while on the tailplane RAMSYS are nearer to experiment (fig.21), these differences being consistent with the wake locations.

The prediction of the vortex core locations from the DERA free wake code are shown in fig.22 for an advance ratio 0.03 and with the tail position 2 shown on the plot. It is seen that the path of the vortices is consistent with the tailplane entering the wake at this speed. Compared to fig.6 it is seen that the vortices are more widely spread about the tailplane, with a greater dominance of horizontal movement.

3 Quartering Flight

3.1 Introduction

The interaction of the main rotor wake with the tail rotor may cause serious performance and handling problems in low speed quartering flight. The most significant conditions occur when the wind is at about 60^o to the longitudinal axis of the helicopter on the side of the advancing blade, i.e. on the left hand side for a main rotor with clockwise rotation. The general layout of the interaction is shown in fig.22.

3.2 Configuration of experiment

The HELIFLOW quartering flight test used a tail rotor designed by GKN-Westland (ref.16) mounted on an independent stand and moved relative to the DERA main rotor rig. The tail rotor could be located at azimuth angles between 0 and 80^o. A spacer in the stand allowed the tail rotor to be in either high or low positions relative to the main rotor, i.e. level with the main rotor hub or 400mm below it respectively. Fig.24 shows the tail rotor on the mounting stand beside the DERA main rotor rig.

The tail rotor was designed to allow rotation in either direction, since it has been found that the less-efficient top-blade-forward direction of rotation is more susceptible to the problem

Tail rotor pitch was selectable over a range –5 to $+30^o$. The tail rotor thrust and torque were measured and recorded on the main rotor rig data acquisition system along with the main rotor controls, forces, moments and strains.

All the quartering flight tests were conducted with the tail rotor operating at 5611 rpm. To obtain the same tip speed for each rotor (147 m/s) the main rotor was operated at the reduced speed of 930 rpm. Higher operating speeds were not used in order to limit the blockage effects due to the size of the tail rotor drive motor , which were still relatively large even for the chosen design conditions.

3.3 Experimental results

Tail rotor and main rotor characteristics were measured with the tail rotor at azimuth positions between zero and 70^o. The main rotor was operated at two thrusts and advance ratio ranging up to 0.13.

Significant interactions were identified for the tail rotor at azimuth positions 50^o and 60^o and so experimental measurements were concentrated on these configurations. Variations with advance ratio of the torque and thrust of the tail rotor at one pitch setting are shown in figures 25 and 26. The values are plotted as the ratio between the value for this value in interaction and the value for the stationary isolate dtail rotor with the same pitch setting.

It is seen that the low position tail rotor with Top-Blade-Aft (TBA) rotation there is a reduction of thrust up to an advance ratio of 0.05 and then a sudden recovery when speed increases to 0.06. In this speed band the low Top-Blade-Forward (TBF) rotor

continues to loose thrust before recovering at a higher advance ratio. The changes are less severe for the high position tail rotors.

Figure 27 shows that the effect applies for all pitch demands. For the TBA tail rotor in low position the thrusts at almost all pitch settings are least for the advance ratio 0.05. The other advance ratios affect different pitches to differing extents, but whatever the pitch demand there would be a sudden reduction in thrust and hence yaw moment when the advance ratio passes through 0.05.

3.4 Comparisons with predictions

In general partners used the same codes for quartering flight analysis as had been used for pitch-up with the addition of tail rotor modelling.

ONERA modified the tail rotor aerofoil characteristics used in the HOST simulation to improve the prediction of the isolated tail rotor characteristics. This was a common experience with all partners, the small scale and large support structure degrading the performance of the experimental tail rotor.

ONERA analysed the rotation and normal speed effects of the interacting vortex on the tail rotor, although it was noted that modification of the model was necessary to achieve vortex intersection with the tail rotor. For the TBA case studied against a range of advance ratio, the vortex rotation gave a smooth transient increase in thrust near 0.06 and the vortex normal speed effect gave a drop in thrust at 0.052 followed by a sudden increase. When combined the two effects indicated the scale and position of the measured phenomenon but over-emphasised the recovery at high advance ratio (fig. 28).

GKN-Westland, ref.17 , used a similar approach of estimating position of vortices near the tail rotor and investigating their effect on an idealised tail rotor model. Predictions for the high position thrusts follow similar trends to the measured data but with rather lower losses. For the low position the interactions are less severe and at a lower advance ratio, deduced to be due to inaccuracy in vortex position.

NLR used a disc model of the tail rotor which did not include the effect of direction of rotation. Comparing the results with the TBA data showed good correlation of the continuing thrust reduction for zero azimuth and also at low speeds for azimuth 60^o. However the sudden recovery at higher advance ratios is not predicted (ref.18).

AGUSTA applied the VSAERO code to the isolated tail rotor and the interacting coupled configuration. Both thrust and torque predictions showed fluctuations of the very similar character to the experimental data, with some variation in absolute level.

ECD, ref.19, calculated the main rotor/tail rotor interactions with CAMRAD II, using the general free wake model for the main rotor and a uniform inflow model for the tail rotor, ref.20. The selected input parameters are a compromise between the low speed and the hover wake model. As a baseline the input data for the low speed model are selected, which are recommended for advance ratios $\geq$ 0.05 approximately, according to the CAMRAD manual. The following modifications of these data are then introduced:

Number of	Heliflow value	manual recommendation	
		low speed	hover
revolutions of wake age	6	$\geq$3	5
revolutions below point where velocity is calculated	6	4	10
wake loop iteration	3	1	3 to 5

Further improvements of the prediction are achieved by using a linear increasing core radius for tip vortices and inboard wake. The core radius equals the blade mean chord after two revolutions.

Eurocopter, ref.21, analysed the test data from the point of view of certification of the controllability of a helicopter. Instead of studying the thrust at a constant pitch, interpolation was used to extract from the data the tail rotor pitch which would be required to maintain a constant 80N thrust. Fig.29 shows the result for tailplane high and low positions. At an advance ratio of 0.05, corresponding to 21kt for a full scale helicopter, 4^o extra pitch is required to maintain thrust. As 14% of control range this would not give acceptable handling characteristics.

4 Conclusions

This paper has described the Heliflow tests conducted in the DERA 24ft wind tunnel and related analyses.

The helicopter fuselage model clearly demonstrated the occurrence of pitch-up. The value of refining the detailed modelling in the analysis methods was demonstrated and generally good agreement was obtained with the experiment, particularly for more rearward tailplane locations.

An independent tail rotor was used with the main rotor in the study of quartering flight. The main rotor/tail rotor interaction was observed clearly, with significant variations of tail rotor torque and thrust. While some analysis methods gave an indication of the speed at which the problem would occur or the severity, no codes gave a full prediction of the phenomenon.

The authors acknowledge the support of the European Commission for this project under Brite/Euram III BRPR-CT96-0206

5 References

1 G Preatoni *Fuselage Geometry and Transducers*, HFLOW/01/AGUSTA/01A, AGUSTA, March 1998.

2 I W Kaynes, R H Markiewicz, K R A Thornton *Description of the DRA Rotor Rig and the 24ft Wind Tunnel for Heliflow* DERA/ASD/CR96353, DERA, November 1996.

3 R H Markiewicz *Detailed Description of the DERA Rotor Rig Hub and the PM1 Rotor Blades for Heliflow,* DERA/MSS5/CR980170/1.0, DERA, June 1998.

4 R H Markiewicz *Description of the wind tunnel tests for task1 and 2 of the CEC Heliflow program* DERA/MSS/MSTR2/CR990069 DERA, May 1999.

5 F De Gregorio *Heliflow Pitch-Up phenomenon characterisation by PIV.* CIRA-TR-LAS-99-098, CIRA, May 1999.

6 N Tino *HELIFLOW results of the hot wire measurements.* CIRA-TR-LAS-99-086, CIRA, May 1999.

7 D Barbagallo, F De Gregorio, N Tino *Helicopter wake investigation by means of PIV and HW measurement techniques.* 9th ISFV, 2000.

8 F De Gregorio, N Tino *HELIFLOW HW and PIV results comparison.* CIRA-TR-LAS-99-211, CIRA, February 2000.

9 I W Kaynes *Review of initial status of codes applied in Heliflow tasks 1 and 2.* DERA/MSS5/CR980304, DERA, July 1998.

10 C Hermans, B S M Renier *NLR report on HELIFLOW task 1 analysis activities. NLR-TR-2000-247, May 2000.*

11 C Arzoumanian *Heliflow task 1 pitch-up.* Eurocopter TN X000 AR 206 F00, March 2000.

12 K Kampa *Heliflow task 1 pitch-up* ECD-TN-D/TA2-2000/0004. April 2000.

13 A Brocklehurst *Analysis of pitch-up tests.* GKN-WHL Report RSG/00/0182, May 2000.

14 G Preatoni *AGUSTA report on Heliflow task 1&2 activities.* AG-100-91-058, May 2000.

15 A Visingardi *Application of the CIRA computer code RAMSYS to the analysis of the pitch-up phenomenon.* CIRA-TR-AEP-00-026, March 2000.

16 A Brocklehurst *Description of the GKN-WHL model tail rotor.* GKN-WHL Report RSG/00/0181, May 2000.

17 A Brocklehurst *Analysis of tail rotor performance in low speed quartering flight.* GKN-WHL Report RSG/00/0180, March 2000.

18 C Hermans, B S M Renier *NLR report on Heliflow task 2 analysis activities.* NLR-TR-2000-248, May 2000.

19 K Kampa Heliflow Task 2: Quartering Flight. ECD-TN-D/TA2-2000/0005, May 2000.

20 W Johnson *A general free wake geometry calculation for wings and rotor.* 51st AHS, May 1995.

21 C Arzoumanian *Heliflow task 2 quartering flight.* Eurocopter TN X000 AR 403 F00, April 2000.

6 Figures

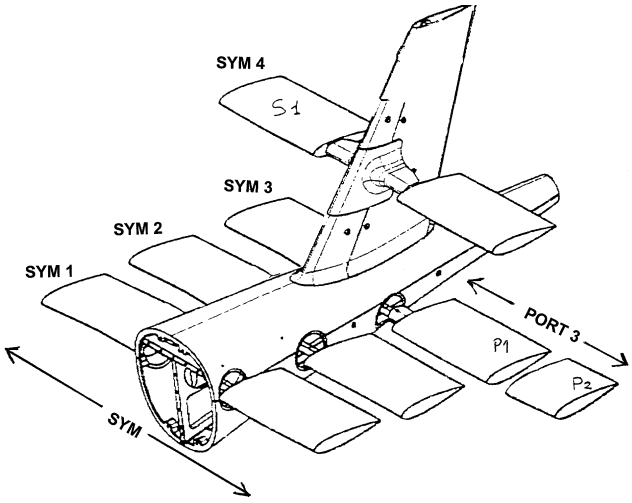

Figure 1 Tailplane configuration options

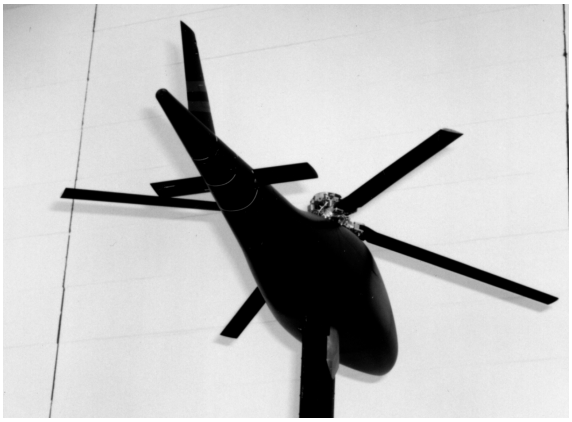

Figure 2 Fuselage and rotor for pitch-up experiment

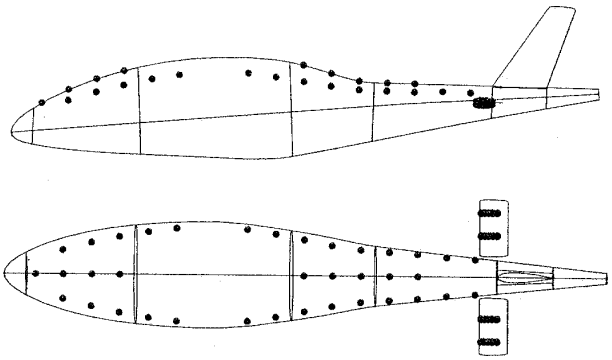

Figure 3 Locations of unsteady pressure transducers

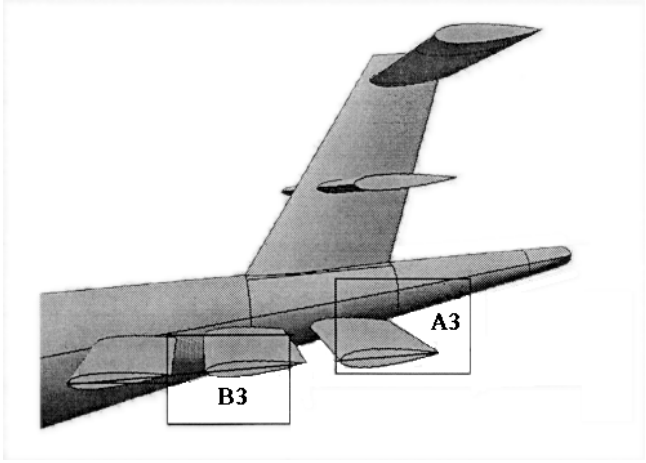

Figure 4 PIV observation zones

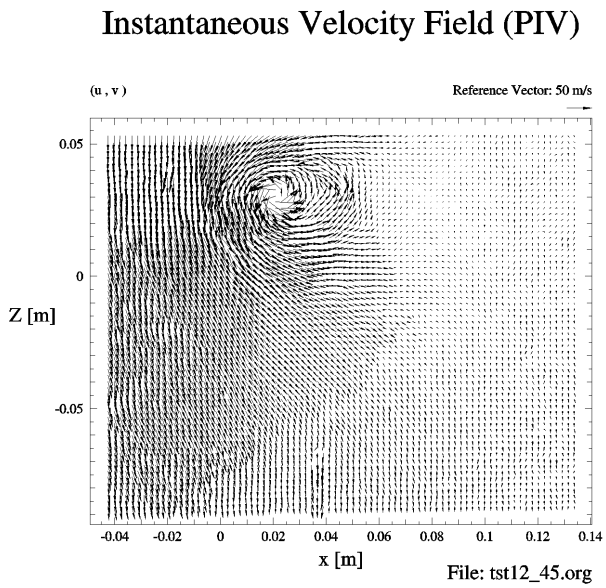

Figure 5 Sample velocity field from PIV

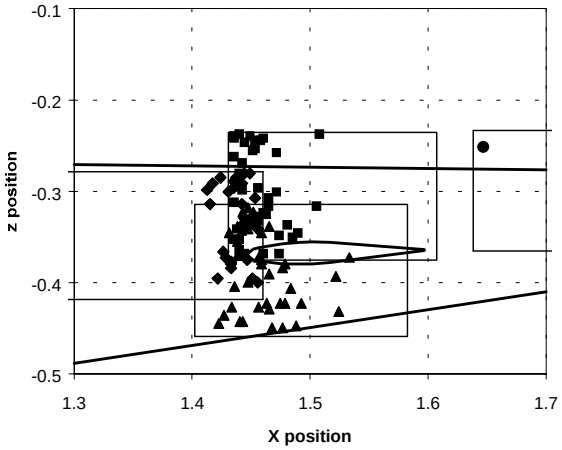

Figure 6 Vortex core locations from PIV for 4 sets of tests at advance ratio 0.03

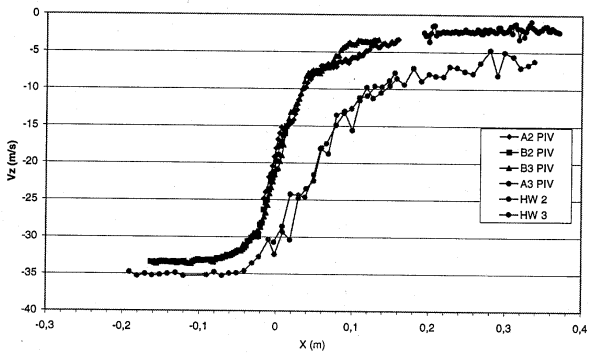

Figure 7 Vertical velocity profiles from PIV and HWA

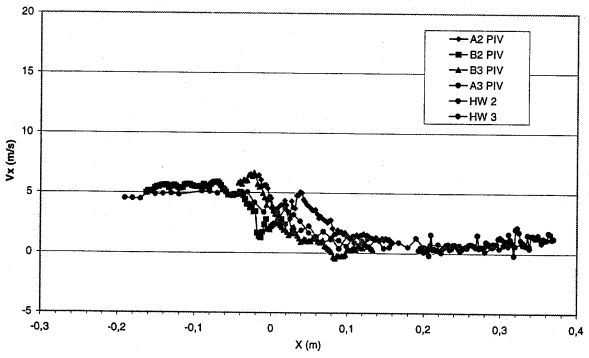

Figure 8 Horizontal velocity profiles from PIV and HWA

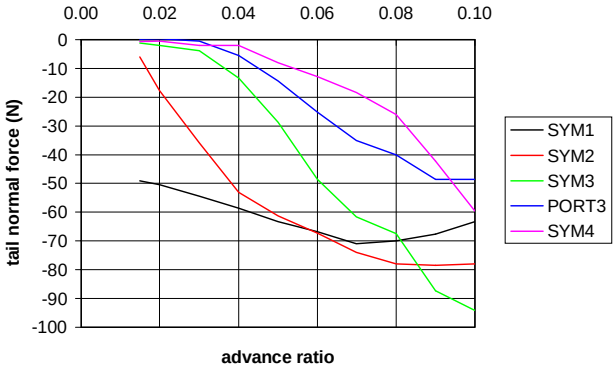

Figure 9 Tailplane normal force versus advance ratio (SYM = total of port and starboard tailplane)

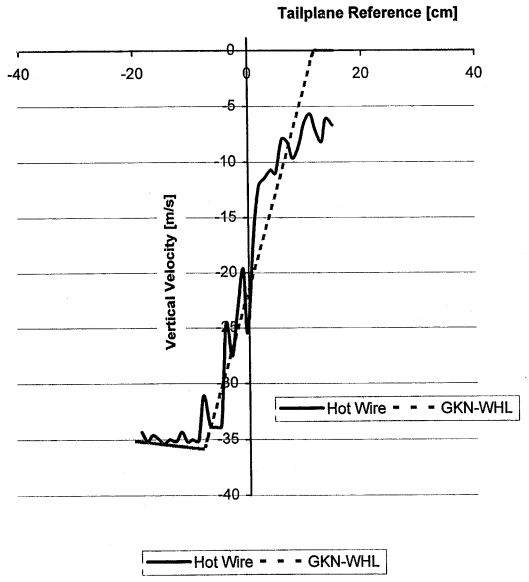

Figure 10 Predicted vertical velocity at tailplane position 2, advance ratio=0.02 (GKN-Westland)

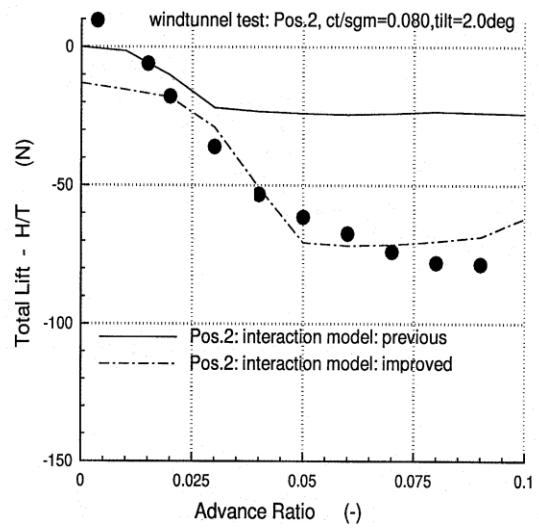

Figure 11 Improvement of tail normal force prediction with interaction model (ECD)

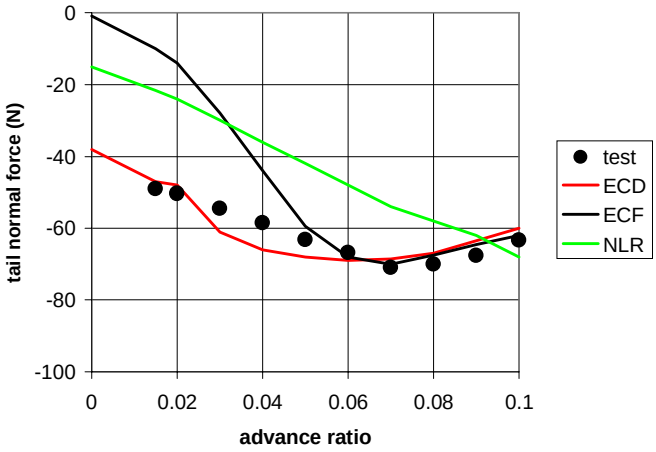

Figure 12 Tail SYM1 total normal force

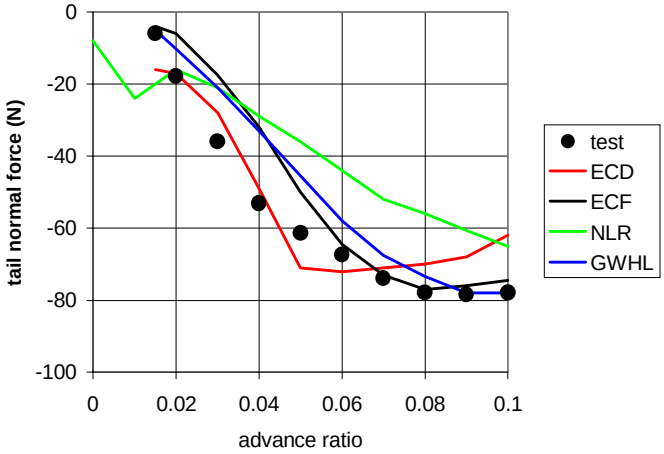

Figure 13 Tail SYM2 total normal force

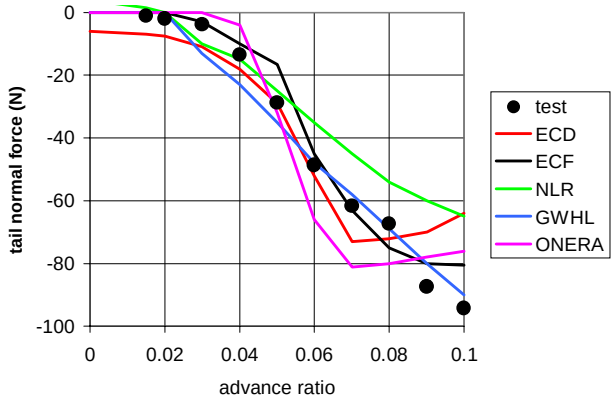

Figure 14 Tail SYM3 total normal force

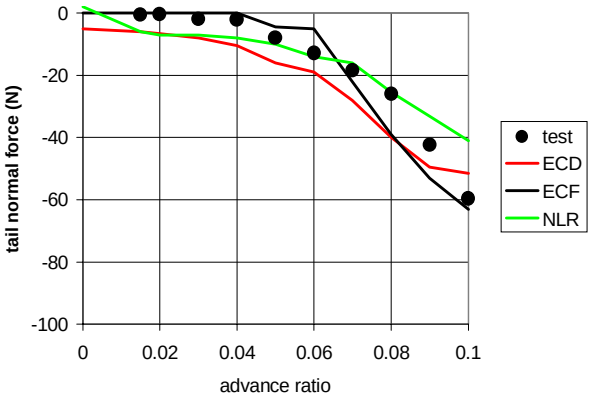

Figure 15 Tail SYM4 total normal force

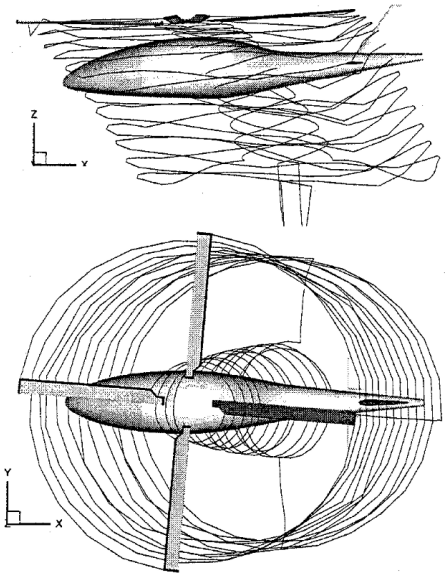

Figure 16 RAMSYS tip vortices, top and side views, μ=0.03

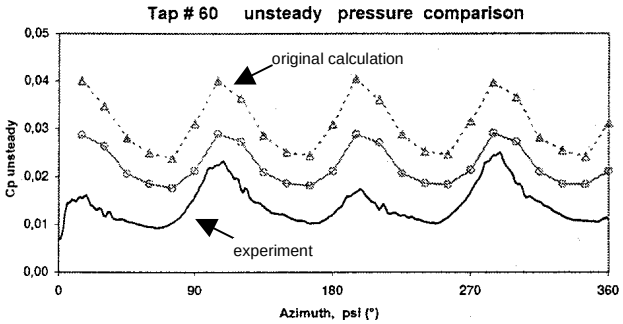

Figure 17 Pressure on tailplane predicted by AGUSTA with RAMSYS, showing experiment, original calculation and calculation with tuned thrust, μ=0.03 tail SYM2

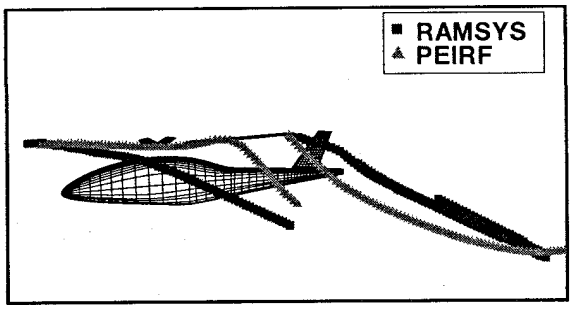

Figure 18 Rotor wake boundaries from PEIRF and RAMSYS, μ=0.10

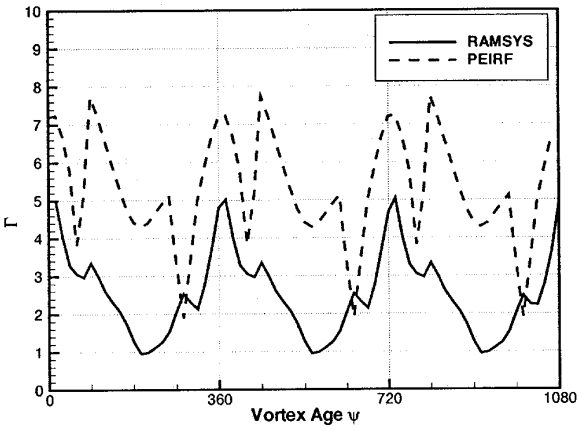

Figure 19 Tip vortex circulation from PEIRF and RAMSYS, μ=0.10

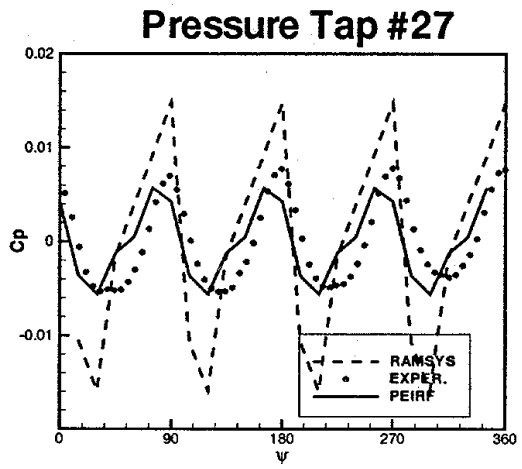

Figure 20 Rear fuselage pressure prediction from PEIRF and RAMSYS, μ=0.10

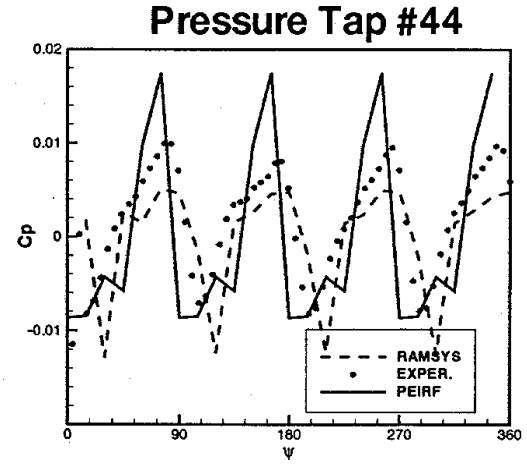

Figure 21 Tailplane upper surface pressure prediction from PEIRF and RAMSYS, μ=0.10

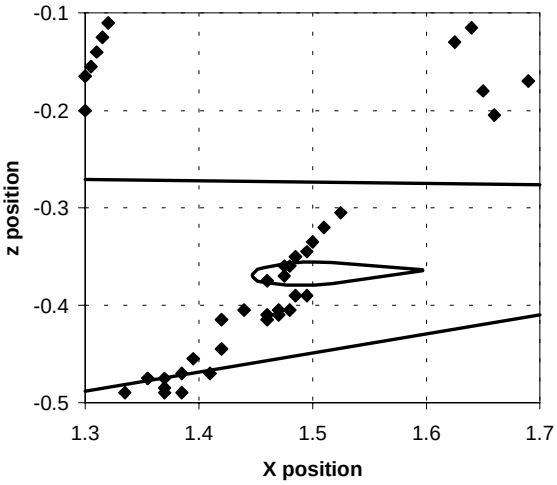

Figure 22 DERA Free Wake vortex locations, μ=0.03, positions shown every 5° blade rotation for one quarter revolution.

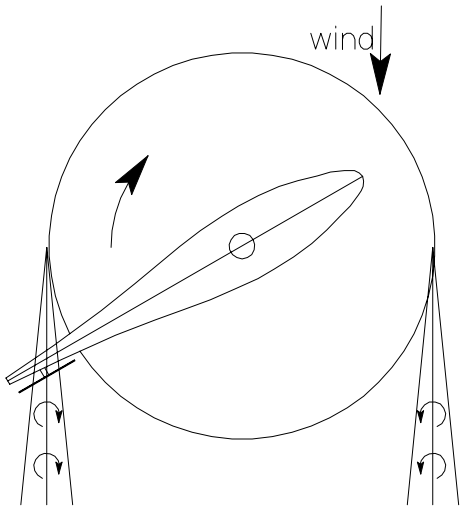

Figure 23 General schematic of quartering flight interaction

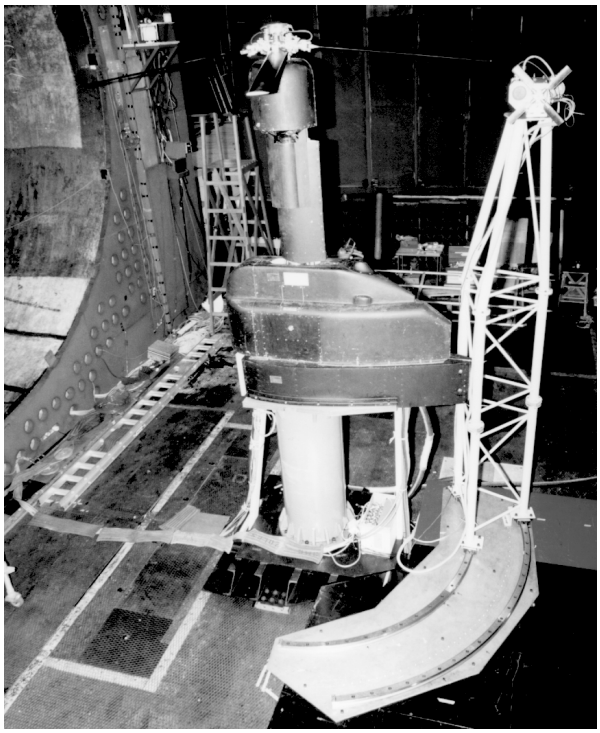

Figure 24 Main rotor and tail rotor mounted in DERA 24ft wind tunnel.

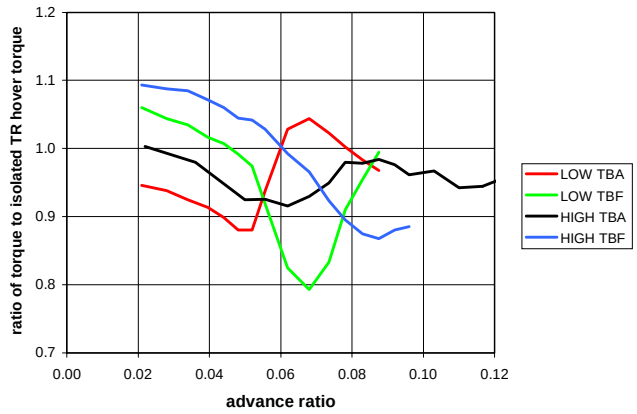

Figure 25 Torque of tail rotor at 60° azimuth position.

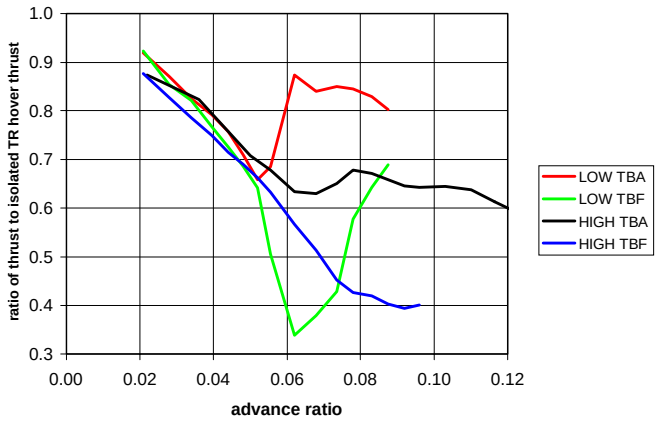

Figure 26 Thrust of tail rotor at 60° azimuth position.

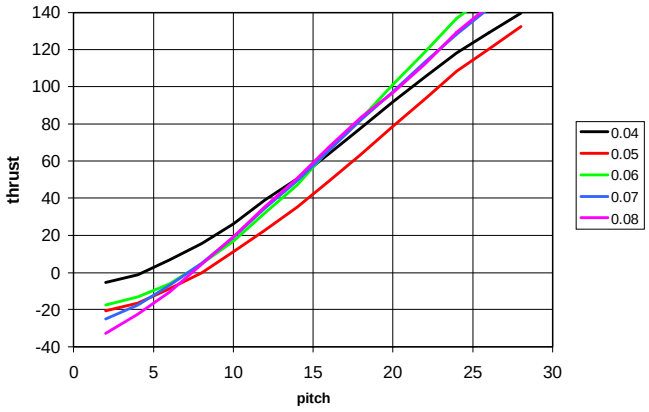

Figure 27 Tail rotor thrust with pitch for a range of advance ratio, low tail rotor TBA at 60° azimuth

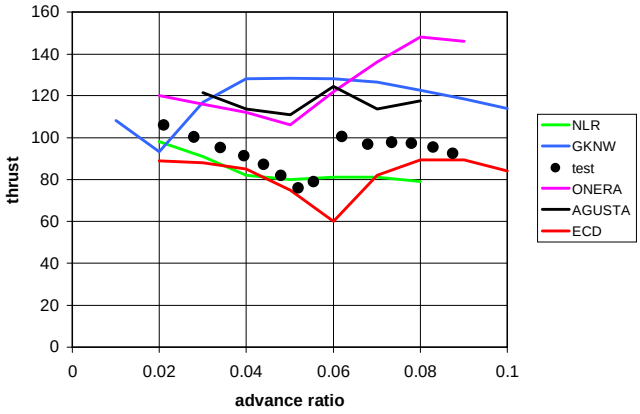

Figure 28 Comparison of predictions with experiment, pitch=20°, low tail rotor TBA at 60° azimuth.

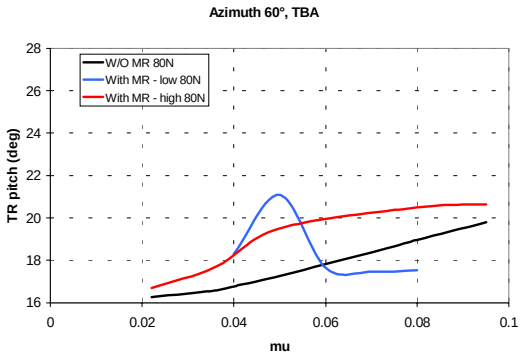

Figure 29 Tail rotor pitch required to maintain constant thrust (60° azimuth, TBA)